

More-Realistic Band Gaps from Meta-Generalized Gradient Approximations: Only in a Generalized Kohn-Sham Scheme

Zeng-hui Yang,¹ Haowei Peng,¹ Jianwei Sun,¹ and John P. Perdew¹

¹*Department of Physics, Temple University, Philadelphia, PA 19122, USA*

(Dated: May 10, 2016)

Unlike the local density approximation (LDA) and the generalized gradient approximation (GGA), calculations with meta-generalized gradient approximations (meta-GGA) are usually done according to the generalized Kohn-Sham (gKS) formalism. The exchange-correlation potential of the gKS equation is non-multiplicative, which prevents systematic comparison of meta-GGA bandstructures to those of the LDA and the GGA. We implement the optimized effective potential (OEP) of the meta-GGA for periodic systems, which allows us to carry out meta-GGA calculations in the same KS manner as for the LDA and the GGA. We apply the OEP to several meta-GGAs, including the new SCAN functional [Phys. Rev. Lett. 115, 036402 (2015)]. We find that the KS gaps and KS band structures of meta-GGAs are close to those of GGAs. They are smaller than the more realistic gKS gaps of meta-GGAs, but probably close to the less-realistic gaps in the band structure of the exact KS potential, as can be seen by comparing with the gaps of the EXX+RPA OEP potential. The well-known grid sensitivity of meta-GGAs is much more severe in OEP calculations.

PACS numbers: 71.15 Mb, 31.15 es

I. INTRODUCTION

Semiconductor devices play an important role in modern technologies, and the rapid development of electronic structure theory methods has made computational design of such devices possible. The band gap and the band structure are undoubtedly the most important properties of semiconductors, since these are the properties that distinguish semiconductors from other periodic systems¹. Computational evaluation of the band gap and the band structure is thus a topic of active research.

The fundamental band gap is a ground-state property, and it is defined as $E_g = I - A$, where I is the ionization energy, and A is the electron affinity. I and A are ground-state energy differences. E_g is also an excited-state property since it is the unbound limit of the exciton series. E_g is very difficult to calculate for periodic systems, since there is no systematic way of adding/removing one electron to/from the solid in a periodic calculation, and the bulk limit can only be approached by the calculation of very big clusters. Many-body methods such as the GW method² calculate E_g and the quasiparticle band structure accurately, but the computational cost is high.

The density-functional theory (DFT)³⁻⁵ is a formally exact electronic structure method for the ground-state energy and electron density with an excellent balance of accuracy and computational efficiency, which is achieved by mapping the real interacting system to a fictitious Kohn-Sham (KS) system of non-interacting electrons with a multiplicative effective exchange-correlation (xc) potential (the functional derivative of the exchange-correlation energy with respect to the density). The exact Kohn-Sham potential yields the exact density but *not* the exact quasi-particle band structure and gap. Though the exact energy functional of the DFT is unknown, there exists a plethora of approximations, which has been ordered into the ‘Jacob’s ladder’⁶ hierarchy. The first and

the second rungs of the Jacob’s ladder are the local density approximation (LDA) and the generalized gradient approximation (GGA), and they severely underestimate the fundamental gap in periodic systems. For periodic systems, KS DFT cannot calculate E_g from its definition, and one commonly approximates E_g with the KS gap $E_g^{\text{KS}} = \epsilon_{\text{LUMO}}^{\text{KS}} - \epsilon_{\text{HOMO}}^{\text{KS}}$, where $\epsilon_{\text{HOMO}}^{\text{KS}}$ and $\epsilon_{\text{LUMO}}^{\text{KS}}$ are the KS orbital energies of the highest occupied orbital and of the lowest unoccupied orbital, respectively. However, E_g^{KS} is not equal to E_g even with the exact functional, due to the derivative discontinuity (DD)⁷. The band gap problem has been an obstacle in the application of DFT to periodic systems.

The generalized Kohn-Sham (gKS)⁸ scheme is a different formulation of the DFT, which allows a non-multiplicative but still Hermitian xc potential operator. The gKS gap $E_g^{\text{gKS}} = \epsilon_{\text{LUMO}}^{\text{gKS}} - \epsilon_{\text{HOMO}}^{\text{gKS}}$ can be a better approximation to E_g than is the KS gap⁹. The third rung of the Jacob’s ladder, the meta-generalized gradient approximation (meta-GGA), is commonly implemented in the gKS scheme according to the method of Neumann, Nobes and Handy (also denoted as gKS in this paper)¹⁰. The gKS meta-GGA band gap of periodic systems improves¹¹ over the KS GGA gaps as expected. In this work we find that, with the recently proposed strongly constrained and appropriately normed (SCAN) functional^{12,13}, the gKS meta-GGA gap corrects about 20%~50% of the difference between the experimental fundamental gap and the GGA KS gap.

Due to the restriction in the functional form of GGA, a GGA cannot perform well for finite systems and periodic systems at the same time.¹⁴ On the other hand, the functional form of meta-GGA can satisfy more exact conditions and has a wider range of applicability than the GGA form. The SCAN functional is a non-empirical functional that satisfies all known exact constraints appropriate to

a semilocal functional, and is expected to perform well for systems with very different kinds of bonds. The computational accuracies of the SCAN functional for many properties improve over those of the GGAs, with only marginal increase of computational cost.¹² We find that SCAN also improves band gaps, but the comparison is between meta-GGA gKS gaps and GGA KS gaps, which are not the same quantity. It is unclear whether the KS gap itself is improved, or just the gKS gap is improved. One needs to do meta-GGA calculations in the KS scheme to be able to have a systematic comparison of the KS band gaps between meta-GGA and GGA.

In the gKS formalism for an orbital functional such as a meta-GGA or hybrid functional, we find the ‘‘optimal variational potential’’, a non-multiplicative self-adjoint operator that minimizes the energy functional with respect to the orbitals. This potential is a differential operator for a meta-GGA and an integral operator for a hybrid functional. In the KS formalism for an orbital functional, we find the optimized effective potential (OEP)^{15,16}, the multiplicative xc potential that minimizes the energy. The OEP meta-GGA yields the KS gap of the meta-GGA, which can be compared directly with the GGA KS gap. With the OEP, the meta-GGA xc potential also becomes comparable with that of the GGA. The OEP meta-GGA has been studied only in finite systems previously.^{17,18}

In this work, we provide the first study of the OEP meta-GGA in periodic systems. We find that the meta-GGA KS gap is not significantly improved over the GGA KS gaps, and the band structure of the OEP meta-GGA is very close to that of the GGA (and presumably to that of the exact KS potential). The xc potential of the meta-GGA has more details than that of the GGA, but the change is not as big as the change between the LDA and the GGA. Though the gKS meta-GGA is known to be sensitive to the real-space grid used in the calculation, we find that the OEP meta-GGA has worse grid sensitivity. The reason for the grid sensitivity is discussed in this work.

Within the gKS implementation of the meta-GGA form, it is possible to fit to energy gaps of solids¹⁹, and the result can be useful for the prediction of gaps²⁰. But the fact that a property can be fitted in DFT is not evidence that it should be, or that other and more appropriate properties will not deteriorate as a result.

II. OEP META-GGA IN PERIODIC SYSTEMS

A. Theory

The meta-GGA xc energy functional has the form

$$E_{xc}[n_{\uparrow}, n_{\downarrow}] = \int d^3r e_{xc}[n_{\uparrow}(\mathbf{r}), n_{\downarrow}(\mathbf{r}), \nabla n_{\uparrow}(\mathbf{r}), \nabla n_{\downarrow}(\mathbf{r}), \tau_{\uparrow}(\mathbf{r}), \tau_{\downarrow}(\mathbf{r})], \quad (1)$$

where e_{xc} is the xc energy density, and n_{σ} and τ_{σ} are the spin density and the kinetic energy density of spin σ respectively. n_{σ} and τ_{σ} are

$$n_{\sigma}(\mathbf{r}) = \frac{1}{\Omega_{\text{BZ}}} \sum_i \int_{\text{BZ}} d^3k \theta_{i\sigma}(\mathbf{k}) |\psi_{i\mathbf{k}\sigma}(\mathbf{r})|^2, \quad (2)$$

$$\tau_{\sigma}(\mathbf{r}) = \frac{1}{2\Omega_{\text{BZ}}} \sum_i \int_{\text{BZ}} d^3k \theta_{i\sigma}(\mathbf{k}) |\nabla \psi_{i\mathbf{k}\sigma}(\mathbf{r})|^2, \quad (3)$$

where Ω_{BZ} is the volume of the first Brillouin zone (BZ), i is the band index, $\psi_{i\mathbf{k}\sigma}$ is the KS orbital normalized in one unit cell, and $\theta_{i\sigma}(\mathbf{k}) = \theta[E_{\text{F}} - \epsilon_{i\mathbf{k}\sigma}]$ is the Heaviside step function, with E_{F} being the Fermi energy, and $\epsilon_{i\mathbf{k}\sigma}$ being the KS orbital energy. The non-interacting kinetic energy density of the Kohn-Sham orbitals is, like the orbitals themselves, a functional of the electron density. The OEP of the meta-GGA is defined by the functional derivative of the xc energy with respect to the density, which is

$$v_{xc,\sigma}(\mathbf{r}) = \frac{\delta E_{xc}}{\delta n_{\sigma}(\mathbf{r})} = \frac{\partial e_{xc}}{\partial n_{\sigma}}(\mathbf{r}) - \nabla \cdot \left[\frac{\partial e_{xc}}{\partial \nabla n_{\sigma}}(\mathbf{r}) \right] + \int d^3r' \frac{\partial e_{xc}}{\partial \tau_{\sigma}}(\mathbf{r}') \frac{\delta \tau_{\sigma}(\mathbf{r}')}{\delta n_{\sigma}(\mathbf{r})}. \quad (4)$$

Eq. (4) can be partitioned into a GGA-like part and a τ -dependent part:

$$v_{xc,\sigma}(\mathbf{r}) = v_{xc,\sigma}^{\text{GGA}}(\mathbf{r}) + v_{xc,\sigma}^{\tau\text{-dep}}(\mathbf{r}). \quad (5)$$

$v_{xc,\sigma}^{\text{GGA}}$ is a multiplicative potential, but $v_{xc,\sigma}^{\tau\text{-dep}}$ does not have a closed form. $v_{xc,\sigma}^{\tau\text{-dep}}$ can be written as

$$v_{xc,\sigma}^{\tau\text{-dep}}(\mathbf{r}) = \frac{1}{\Omega_{\text{BZ}}} \sum_i \int_{\text{BZ}} d^3k \iint_{V_{\text{cell}}} d^3r' d^3r'' \frac{\partial e_{xc}}{\partial \tau_{\sigma}}(\mathbf{r}') \times \left[\frac{\delta \tau_{\sigma}(\mathbf{r}')}{\delta \psi_{i\mathbf{k}\sigma}(\mathbf{r}'')} \frac{\delta \psi_{i\mathbf{k}\sigma}(\mathbf{r}'')}{\delta n_{\sigma}(\mathbf{r})} + \text{c.c.} \right]. \quad (6)$$

On one hand, the gKS meta-GGA potential operator is obtained by multiplying both side of Eq. (6) by $\delta n_{\sigma}(\mathbf{r})/\delta \psi_{i\mathbf{k}'\sigma'}(\mathbf{r}_1) + \text{c.c}$ and integrating over \mathbf{r} :

$$v_{xc,\sigma}^{\tau\text{-dep}}(\mathbf{r}) \psi_{i\mathbf{k}\sigma}(\mathbf{r}) = -\frac{1}{2} \nabla \cdot \left[\frac{\partial e_{xc}}{\partial \tau_{\sigma}}(\mathbf{r}) \nabla \psi_{i\mathbf{k}\sigma}(\mathbf{r}) \right] \equiv \hat{v}_{xc,\sigma}^{\text{gKS}} \psi_{i\mathbf{k}\sigma}(\mathbf{r}). \quad (7)$$

On the other hand, inserting

$$\frac{\delta \psi_{i\mathbf{k}\sigma}(\mathbf{r}'')}{\delta n_{\sigma}(\mathbf{r})} = \int_{V_{\text{cell}}} d^3r_1 \frac{\delta \psi_{i\mathbf{k}\sigma}(\mathbf{r}'')}{\delta v_{s,\sigma}(\mathbf{r}_1)} \frac{\delta v_{s,\sigma}(\mathbf{r}_1)}{\delta n_{\sigma}(\mathbf{r})}, \quad (8)$$

where v_s is the KS potential, into Eq. (6) yields the OEP integral equation for $v_{\text{XC},\sigma}^{\tau\text{-dep}}$:

$$\begin{aligned} & \int_{V_{\text{cell}}} d^3r v_{\text{XC},\sigma}^{\tau\text{-dep}}(\mathbf{r}) \frac{\delta n_\sigma(\mathbf{r})}{\delta v_{s,\sigma}(\mathbf{r}_1)} + \text{c.c.} \\ &= \frac{1}{\Omega_{\text{BZ}}} \sum_i \int_{\text{BZ}} d^3k \iint_{V_{\text{cell}}} d^3r' d^3r'' \frac{\partial e_{\text{XC}}}{\partial \tau_\sigma}(\mathbf{r}') \frac{\delta \tau_\sigma(\mathbf{r}')}{\delta \psi_{i\mathbf{k}\sigma}(\mathbf{r}'')} \frac{\delta \psi_{i\mathbf{k}\sigma}(\mathbf{r}'')}{\delta v_{s,\sigma}(\mathbf{r}_1)} \end{aligned} \quad (9)$$

Though a direct solution for the OEP is possible^{18,21}, it is both computationally expensive and numerically unstable. The common practice is to approximate the solution of Eq. (9). Ref. 17 employed the local-Hartree-Fock (LHF)²² approximation to derive approximated $v_{\text{XC},\sigma}^{\tau\text{-dep}}$ of meta-GGA for finite systems. Here we do the derivation with the effective local potential (ELP)^{23,24} approximation. The ELP is equivalent to the LHF and the common-energy-denominator approximation (CEDA)^{25,26}, and the Krieger-Li-Iafrate (KLI)²⁷ approximation is their simplification.

The ELP minimizes the matrix norm of the commutator $S_\sigma = [\hat{D}_\sigma, \hat{\rho}_\sigma]$, where $\hat{D}_\sigma = v_{\text{XC},\sigma}^{\tau\text{-dep}} - \hat{v}_{\text{XC},\sigma}^{\text{gKS}}$, and $\hat{\rho}_\sigma = \frac{1}{\Omega_{\text{BZ}}} \sum_i \int d^3k \theta_{i\sigma}(\mathbf{k}) |\psi_{i\mathbf{k}\sigma}\rangle \langle \psi_{i\mathbf{k}\sigma}|$ is the spin density matrix. $\hat{\rho}_\sigma$ becomes valid for both the KS and the gKS system when $S_\sigma = 0$. S_σ is minimized when $\delta S_\sigma / \delta v_{\text{XC},\sigma}^{\tau\text{-dep}}(\mathbf{r}) = 0$, which yields the ELP approximation of $v_{\text{XC},\sigma}^{\tau\text{-dep}}$:

$$\begin{aligned} v_{\text{XC},\sigma}^{\tau\text{ELP}}(\mathbf{r}) &= \\ & \frac{1}{2\Omega_{\text{BZ}} n_\sigma(\mathbf{r})} \int_{\text{BZ}} d^3k \left\{ \sum_i \theta_{i\sigma}(\mathbf{k}) \psi_{i\mathbf{k}\sigma}^*(\mathbf{r}) \hat{v}_{\text{XC},\sigma}^{\text{gKS}} \psi_{i\mathbf{k}\sigma}(\mathbf{r}) \right. \\ & + \frac{1}{\Omega_{\text{BZ}}} \int_{\text{BZ}} d^3k' \sum_{ij} \theta_{i\sigma}(\mathbf{k}) \theta_{j\sigma}(\mathbf{k}') \psi_{i\mathbf{k}\sigma}^*(\mathbf{r}) \psi_{j\mathbf{k}'\sigma}(\mathbf{r}) \\ & \left. \times \left\langle \psi_{j\mathbf{k}'\sigma} \left| \hat{D}_\sigma \right| \psi_{i\mathbf{k}\sigma} \right\rangle \right\} + \text{c.c.} \end{aligned} \quad (10)$$

The ELP approximates the OEP in a least-squares sense²⁴.

Ref. 24 shows that the ELP approximation is equivalent to the CEDA, which reduces to the KLI approximation by setting $i = j$ in Eq. (10)²⁵. If only the first term of Eq. (10) is kept, one obtains the so-called Slater approximation²⁸.

B. Implementation in the BAND code

The most efficient methods for calculating periodic systems are pseudopotential methods with plane-wave basis sets, with the widely used PAW method as an extension^{29,30}, but the OEP is hard to implement in such codes. The sum over bands in Eq. (10) also includes the core bands, which are not directly available in pseudopotential codes. Furthermore, the OEP is inherently incompatible with the PAW formalism. The charge density in

the PAW formalism is composed of the pseudo-charge-density, the on-site all-electron density, and the on-site pseudo-charge-density^{29,30}, and the xc energy and potential are partitioned into three parts accordingly, with each part only depending on the corresponding part of the density. However, the OEP of meta-GGA is hard to partition this way. Due to these obstacles, we implement the OEP meta-GGA in the BAND code³¹⁻³⁵.

BAND is an all-electron DFT code for periodic systems. It uses atom-centered numerical functions as the basis set. All the real-space integrations are done numerically on a Becke fuzzy-cell grid³⁶. The BZ is discretized with the commonly used Monkhorst-Pack grid³⁷, so the \mathbf{k} -integrations of Eq. (10) become sums over \mathbf{k} -points in the irreducible Brillouin zone (IBZ):

$$\frac{1}{\Omega_{\text{BZ}}} \int d^3k g_{i\sigma}(\mathbf{k}) \theta_{i\sigma}(\mathbf{k}) = \frac{1}{N_G} \sum_{\tilde{\mathbf{k}}} \sum_{\hat{S}} w_{\tilde{\mathbf{k}}} f_{i\tilde{\mathbf{k}}\sigma} g_{i\sigma}(\hat{R}^{-1}\tilde{\mathbf{k}}) \quad (11)$$

where $g_{i\sigma}(\mathbf{k})$ is the contribution to the integral from the orbital $\psi_{i\mathbf{k}\sigma}$, $f_{i\tilde{\mathbf{k}}\sigma}$ is the occupation number, $w_{\tilde{\mathbf{k}}}$ is the weight of the \mathbf{k} -point times the \mathbf{k} -space integration weight in BAND³², N_G is the total number of symmetry operations, $\hat{S} = \{\hat{R}, \mathbf{t}\}$ is the space-group symmetry operator, and \hat{R} is the rotational part of \hat{S} .

The \hat{D}_σ matrix elements in Eq. (10) vanish for $\mathbf{k} \neq \mathbf{k}'$, since \hat{D}_σ has the periodicity of the unit cell. Eq. (10) is implemented in the BAND code as

$$\begin{aligned} v_{\text{XC},\sigma}^{\tau\text{ELP}}(\mathbf{r}) &= \\ & \frac{1}{N_G n_\sigma(\mathbf{r})} \sum_{\tilde{\mathbf{k}}} \sum_{\hat{S}} \sum_i w_{\tilde{\mathbf{k}}} f_{i\tilde{\mathbf{k}}\sigma} \\ & \times \Re \left\{ -\frac{1}{2} \psi_{i\tilde{\mathbf{k}}\sigma}^*(\mathbf{r}) \left[\nabla_{\mathbf{r}} \frac{\partial e_{\text{XC}}}{\partial \tau_\sigma}(\mathbf{r}) \cdot \hat{R}^{-1} \nabla_{\mathbf{r}'} \psi_{i\tilde{\mathbf{k}}\sigma}(\mathbf{r}') \right]_{\mathbf{r}'=\hat{S}\mathbf{r}} \right. \\ & + \frac{\partial e_{\text{XC}}}{\partial \tau_\sigma}(\mathbf{r}) \text{tr} \left\{ \hat{R}^{-1} \cdot \left[\nabla_{\mathbf{r}'} \otimes \nabla_{\mathbf{r}'} \psi_{i\tilde{\mathbf{k}}\sigma}(\mathbf{r}') \cdot \hat{R} \right] \Big|_{\mathbf{r}'=\hat{S}\mathbf{r}} \right\} \\ & \left. + \sum_j f_{j\tilde{\mathbf{k}}\sigma} \psi_{i\tilde{\mathbf{k}}\sigma}^*(\hat{S}\mathbf{r}) \psi_{j\tilde{\mathbf{k}}\sigma}(\hat{S}\mathbf{r}) (I_{ij\tilde{\mathbf{k}}\sigma} - J_{ij\tilde{\mathbf{k}}\sigma}) \right\}, \end{aligned} \quad (12)$$

where I and J are

$$I_{ij\tilde{\mathbf{k}}\sigma} = \int_{V_{\text{cell}}} d^3r \psi_{i\tilde{\mathbf{k}}\sigma}^*(\mathbf{r}) v_{\text{XC},\sigma}^{\tau\text{ELP}}(\mathbf{r}) \psi_{j\tilde{\mathbf{k}}\sigma}(\mathbf{r}), \quad (13)$$

$$J_{ij\tilde{\mathbf{k}}\sigma} = \frac{1}{2} \int_{V_{\text{cell}}} d^3r \frac{\partial e_{\text{XC}}}{\partial \tau_\sigma}(\mathbf{r}) \nabla \psi_{i\tilde{\mathbf{k}}\sigma}^*(\mathbf{r}) \cdot \nabla \psi_{j\tilde{\mathbf{k}}\sigma}(\mathbf{r}), \quad (14)$$

and $\nabla_{\mathbf{r}'} \otimes \nabla_{\mathbf{r}'} \psi_{i\tilde{\mathbf{k}}\sigma}(\mathbf{r}')$ denotes the Hessian matrix of $\psi_{i\tilde{\mathbf{k}}\sigma}$. The integrals are done as discrete sums on the real-space grid. The $I_{ij\tilde{\mathbf{k}}\sigma}$ depend on $v_{\text{XC},\sigma}^{\tau\text{ELP}}$, which is unknown beforehand. They can be determined by solving linear equations¹⁷, but this is costly for periodic systems. Instead, we determine the I integrals and $v_{\text{XC},\sigma}^{\tau\text{ELP}}$ iteratively by the following steps:

1. Set the I integrals to 0.
2. Calculate $v_{\text{XC},\sigma}^{\tau\text{ELP}}$ with Eq. (12) using the I integrals of the last iteration.
3. Calculate the I integrals using the new $v_{\text{XC},\sigma}^{\tau\text{ELP}}$.
4. Repeat step 2 and 3 if $\int d^3r \left| v_{\text{XC},\sigma}^{\tau\text{ELP}(i)}(\mathbf{r}) - v_{\text{XC},\sigma}^{\tau\text{ELP}(i-1)}(\mathbf{r}) \right| > \mathcal{T}$, where i is the iteration count, and \mathcal{T} is the error tolerance.

$v_{\text{XC},\sigma}^{\tau\text{ELP}}$ is only determined up to an additive constant c , since $v_{\text{XC},\sigma}^{\tau\text{ELP}} + c$ yields the same band structure. c has to be fixed for determining the convergence. The I integrals contain $v_{\text{XC},\sigma}^{\tau\text{ELP}}$, so their values include c . We fix c by requiring that the term of $v_{\text{XC},\sigma}^{\tau\text{ELP}}$ containing the I integrals averages to 0, i.e. the constant c is determined by

$$\frac{1}{V_{\text{cell}}} \int_{V_{\text{cell}}} d^3r \frac{1}{N_G n_{\sigma}(\mathbf{r})} \sum_{\mathbf{k}} \sum_{\hat{S}} \sum_i w_{\mathbf{k}} f_{i\mathbf{k}\sigma} \sum_j f_{j\mathbf{k}\sigma} \times \psi_{i\mathbf{k}\sigma}^*(\hat{S}\mathbf{r}) \psi_{j\mathbf{k}\sigma}(\hat{S}\mathbf{r}) \left(I_{ij\mathbf{k}\sigma} + c\delta_{ij} \right) = 0 \quad (15)$$

In practice, the iterative procedure converges after 200 iterations on average for $\mathcal{T} = 10^{-10}$.

Ref. 26 finds that the total energies and orbital energies obtained from CEDA and KLI are very close for atoms and molecules. We find that the same is true for periodic systems. The ELP is equivalent to the CEDA²⁴, and its total energy is always lower than that of the KLI, but the total energy differences and the KS gap differences of the materials in Table I between that of the ELP and that of the KLI are at most 1 meV. Since the improvement of the ELP over the KLI is insignificant, we only report the KLI results in the following.

III. RESULTS

We calculate the KS and gKS gaps of 20 semiconductors and insulators with the SCAN, meta-GGA made simple 2 (MS2)^{38,39}, meta-GGA made very simple (MVS)⁴⁰ and TPSS⁴¹ meta-GGAs and the PBE⁴² GGA, and the results are collected in Table I. Ge, CdO, and InN are not listed since their calculated gaps vanish. All the calculations are done with the TZ2P basis set⁴³. A $9 \times 9 \times 9$ Monkhorst-Pack \mathbf{k} -grid³⁷ is used for most of the materials except InN, CdS and CdSe, for which a $9 \times 9 \times 5$ \mathbf{k} -grid is used. We find that the OEP meta-GGA is sensitive to the real-space grid, and large grids are used to ensure convergence. The details of the grid problem are discussed in Section IV. Though GGA and gKS meta-GGA converge properly with smaller grids, we use the same grid as the OEP meta-GGA, so that the results are comparable.

The scalar relativistic effect is included in the calculations by the ZORA⁴⁴ method. We ignore the spin-orbit

coupling since the effect is small (0.03 eV for InP). The relativistic effect is implicitly included through the pseudopotential in planewave codes, but it needs to be explicitly included in BAND. We find that the scalar relativistic effect has a big impact on the KS and gKS gaps, since it shifts down the orbital energies of s -type bands, such as the lowest conduction band of GaAs⁴⁵. The change in the KS and gKS gaps due to the scalar relativistic effect can be as big as 0.7 eV (GaAs).

Figs. 1 and 2 compare the OEP of SCAN meta-GGA and the LDA and the PBE xc potentials for the Ne atom and bulk Si, respectively. The exact xc potential of the Ne atom⁴⁶ is plotted as a reference. The exact xc potential of Ne has a bump between the two shells of the charge density. The v_{XC} of LDA does not have this feature. The v_{XC} 's of PBE and SCAN both have this bump, and they are roughly in the same position as that of the exact v_{XC} , but these v_{XC} 's are shallower than the exact v_{XC} . The v_{XC} 's of SCAN also have a few small bumps that are not in the exact v_{XC} . In the asymptotic region, the exact v_{XC} decays as $-1/r$, and the v_{XC} 's of all the semi-local functionals decay exponentially. Fig. 1 shows that the v_{XC} of SCAN has the same decay as that of LDA and PBE. For periodic systems, there is no asymptotic region, and the approximated v_{XC} 's of bulk Si in Fig. 2 can be expected to be closer to the exact v_{XC} than those in Fig. 1. In Fig. 2, the v_{XC} of SCAN are similar to the v_{XC} of PBE, and they only differ in small details. Similar to Fig. 1, the v_{XC} 's of SCAN for bulk Si also have small bumps. Though the meta-GGA is a higher rung functional on the Jacob's ladder than the GGA, the improvement in v_{XC} is small going from GGA to meta-GGA, unlike going from LDA to GGA. The differences between the KS meta-GGA gaps and the PBE gaps in Table I are small as a consequence.

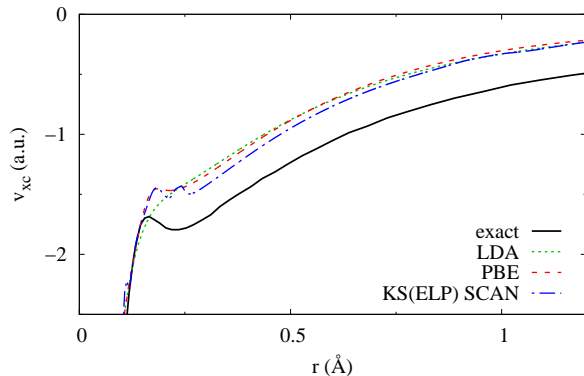


FIG. 1. (color online) Comparison of v_{XC} 's of the Ne atom for SCAN, LDA, and GGA. The exact v_{XC} is from Ref. 46.

The band structures of Si and GaAs calculated with PBE and SCAN are plotted in Figs. 4 and 5. The KS(KLI) SCAN band structure is very close to the PBE band structure, due to the corresponding v_{XC} being similar to the PBE v_{XC} . The gKS SCAN band structure has the same overall shape as that of the PBE and the

Material	Exp.	LDA	PBE	HSE	SCAN			MS2			MVS			TPSS
					gKS	KS(KLI)	Δ_{XC}	gKS	KS(KLI)	Δ_{XC}	gKS	KS(KLI)	Δ_{XC}	
Si	1.17	0.60	0.71	1.11	0.97	0.78	0.19	1.20	0.80	0.41	1.04	0.72	0.32	0.80
InP	1.42	0.50	0.72	1.52	1.06	0.77	0.29	1.14	0.81	0.34	1.99	1.09	0.89	0.86
GaAs	1.52	0.30	0.53	1.41	0.8	0.45	0.34	0.94	0.48	0.46	2.15 ^a	1.26	N/A	0.68
BAs	1.60 ^d	1.21	1.26	1.71	1.51	1.32	0.19	1.63	1.33	0.30	1.56	1.16	0.40	1.26
CdSe	1.73	0.44	0.71	1.66	1.10	0.76	0.33	1.06	N/A ^b	N/A	2.14	0.50	1.64	0.92
BP	2.10	1.36	1.43	1.79	1.74	1.52	0.22	1.94	1.49	0.46	1.64	1.42	0.22	1.48
GaP	2.35	1.53	1.69	2.09	1.94	1.72	0.21	1.97	1.73	0.24	2.23	1.74	0.49	1.74
CdS	2.48	0.96	1.23	2.27	1.62	1.20	0.42	1.60	1.27	0.33	2.39	1.50	0.88	1.43
β -GaN	3.17	1.70	1.69	2.97	2.03	1.84	0.20	1.69	1.70	-0.01	2.50	1.89	0.62	1.60
ZnS	3.72	1.87	2.12	3.32	2.63	2.16	0.47	2.52	2.08	0.45	3.35	N/A ^b	N/A	2.30
C ^c	5.50	4.14	4.17	4.94	4.58	4.26	0.32	4.79	4.16	0.62	4.15	4.06	0.09	4.20
BN	6.20	4.42	4.53	5.39	5.04	4.73	0.30	5.01	4.56	0.45	5.14	4.58	0.56	4.54
CaO	6.93	3.62	3.75	5.30	4.29	3.78	0.50	4.13	N/A ^b	N/A	4.56	3.51	1.05	3.89
MgO	7.90	4.70	4.74	6.46	5.62	4.80	0.82	5.20	5.47	-0.27	6.05	4.58	1.47	4.86
NaCl	8.97	4.70	5.08	6.42	5.86	5.25	0.61	5.85	6.51	-0.66	6.61	4.68	1.93	5.43
LiF	13.6	8.84	9.04	11.4	9.97	9.11	0.86	9.50 ^a	9.84	N/A	10.64	8.77	1.86	9.19
solid Ar	14.3	8.44	8.92	10.33	9.91	8.89	1.02	9.95	9.36	0.58	10.98	9.19	1.80	9.56
MAE		2.08	1.90	0.88	1.41	1.84		1.28	1.63		1.13	1.89		1.76
MARE		0.46	0.40	0.13	0.27	0.38		0.26	0.35		0.19	0.36		0.36

^a converged to the wrong ground state

^b not converged

^c diamond

^d GW gap

TABLE I. Calculated KS/gKS gaps and the derivative discontinuities ($\Delta_{XC} = E_g^{gKS} - E_g^{KS(KLI)}$). All energies are in eV. The experimental gaps are from Ref. 47. The BAs GW gap is from Ref. 48. The mean absolute errors (MAE) and mean absolute relative error (MARE) for the band gaps are listed. HSE^{49–51} gaps calculated with the VASP^{30,52–55} code are also listed for reference. The PBE and SCAN gaps of Ge, CdO, and InN are vanishing, so they are not listed. Their experimental gaps are 0.74 eV, 0.84 eV, and 1.95 eV, respectively. Their HSE gaps are 0.65 eV, 0.94 eV, and 0.77 eV, respectively. The KS(KLI) TPSS results are not listed as most calculations fail to converge.

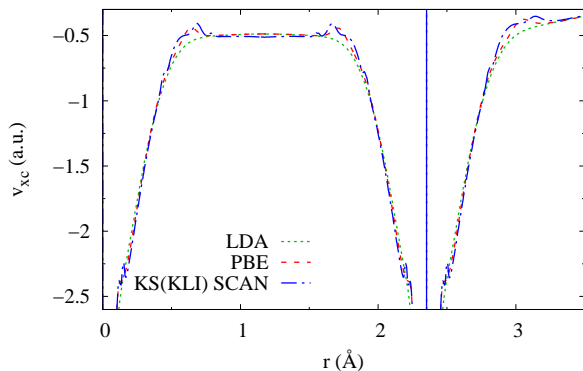


FIG. 2. (color online) Comparison of v_{XC} 's of bulk Si along the Si-Si bond for SCAN, LDA, and GGA. The Si atoms are located at $r = 0$ and $r = 2.35\text{\AA}$. The vertical dashed line is a numerical artifact and does not affect the band structure.

KS(KLI), and the main difference is in the band gap.

Though the gKS meta-GGA band gaps improve over the PBE gaps in general, it is disappointing that gKS meta-GGA gaps for Ge, InN, and CdO still vanish. However, it is possible for meta-GGAs to open the gap for

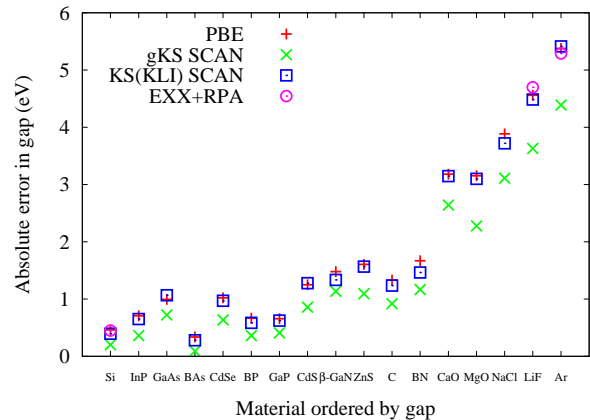


FIG. 3. The absolute errors of PBE, KS(KLI) SCAN, and gKS SCAN (comparing with the experimental gap) in the band gap. The EXX+RPA OEP gaps for Si, LiF and Ar, from Ref. 56, can be considered very close to the gaps for the corresponding exact KS potential.

gapless materials in GGA. gKS SCAN has⁵⁷ a 0.4 eV gap for β -MnO₂, which is gapless in GGA, and the value is close to the experimental value 0.3 eV. The M06L

metaGGA was reported to open the gap of Ge at 0.14 eV.^{11,58}

The improvement of the band gap occurs since, unlike the KS gap, the gKS gap is an approximation to the fundamental gap of the meta-GGA. A Janak-type⁵⁹ theorem has been proven for the OEP⁹, and it states that the gKS gap approximately equals the fundamental gap for the same functional, assuming fixed orbitals. This assumption does not apply to finite systems, but it is true for periodic systems, since the charge density and the orbitals of a periodic system undergo only an infinitesimal change when the number of electrons changes by one.

GGA band gaps should be compared with the OEP meta-GGA band gaps for a fair comparison between approximated functionals, since the OEP meta-GGA band gap is the KS gap. The SCAN functional is the only functional that satisfies all the known exact conditions, but the KS(KLI) SCAN gaps do not have significant improvements over the PBE gaps. This is probably due to the fact that the GGA and SCAN OEP gaps closely approximate the exact KS gap, which underestimates the fundamental gap. This has been illustrated in Fig. 3, where the errors of the EXX+RPA(OEP) KS gaps⁵⁶ are also plotted. EXX+RPA (exact exchange plus random phase approximation for correlation) is a high-level (fifth rung) method, and its OEP gaps are expected to be very close to those of the corresponding exact KS potential. Fig. 3 shows that both PBE and KS SCAN gaps are already good approximations to the exact KS gap.

Some of the gKS band gaps of MS2 and TPSS are smaller than the corresponding OEP band gaps. We do not find this behavior in other functionals. Many of the KS(KLI) TPSS calculations fail to converge. This is probably a numerical issue in the calculation of $\nabla(\partial e_{xc}/\partial\tau_\sigma)$, due to the complicated functional form of TPSS.

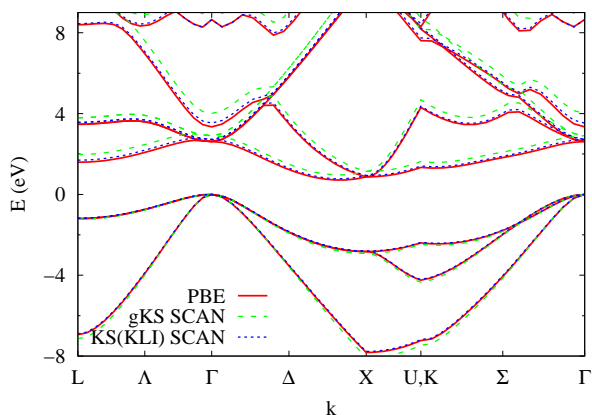


FIG. 4. (color online) The band structure of Si calculated with PBE, gKS SCAN, and KS(KLI) SCAN.

The energy functional of the exact DFT has derivative discontinuities Δ_{xc} at integer electron numbers⁷, where $\Delta_{xc} = E_g - E_g^{KS}$. The exact KS potential jumps up by

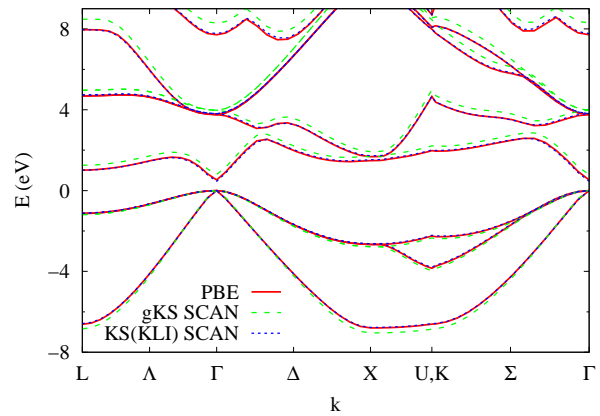


FIG. 5. (color online) The band structure of GaAs calculated with PBE, gKS SCAN, and KS(KLI) SCAN.

the positive constant Δ_{xc} as the electron number crosses the value that makes the solid electrically neutral. LDA and GGA miss much or all of the derivative discontinuity due to the convexity of the approximated energy functional⁶⁰, and they underestimate the gap as a consequence. In periodic systems, such discontinuities are only visible at band gaps. Though the derivative discontinuity has been thoroughly studied for atoms and molecules, it is difficult to obtain for periodic systems, since I and A cannot be calculated directly.

With the OEP meta-GGA provided in this work, we are able to estimate the Δ_{xc} of solids. E_g can be approximated by the derivative gap $E_g^{\text{deriv}} = \partial E/\partial N|_{N_+} - \partial E/\partial N|_{N_-}$, which is equal to the gKS meta-GGA gap^{9,60,61}. E_g^{KS} is the OEP meta-GGA gap. The results are shown in Table I.

Comparison of the Δ_{xc} 's of meta-GGAs with the exact Δ_{xc} is impossible for periodic systems, since no exact KS potential is available. However, Ref. 62 provides an OEP of the GW method of bulk Si, and its Δ_{xc} can be seen as a good approximation to the exact Δ_{xc} . The Δ_{xc} of bulk Si in Ref. 62 is 0.58 eV, which is larger than that of all the meta-GGAs in Table I. This is not unexpected because the meta-GGA's tested in this work are not exact for $I - A$ in a solid.

IV. REAL-SPACE GRID DEPENDENCY

The gKS meta-GGA requires a larger real-space integration grid than GGA⁶³, and this is caused by the sharp variation in regions far away from nuclei of quantities containing τ , such as $z = \tau^W/\tau$ used in TPSS, and $\alpha = (\tau - \tau^W)/\tau_0$ used in SCAN, MS2 and MVS, where $\tau^W = |\nabla n|^2/(8n)$ is the von Weizsäcker kinetic energy density, and $\tau_0 = (3/10)(3\pi^2)^{2/3}n^{5/3}$ is the kinetic energy density of the uniform electron gas. The Becke fuzzy-cell grid is used as the real-space integration grid in most of the DFT codes. It is constructed by combining atom-

Material	solid Ar	LiF	NaCl	MgO	CaO	BN	C ^a	ZnS	β -GaN	CdS	GaP	BP	CdSe	BA5	GaAs	InP	Si
N_r	69	169	82	74	87	74	65	153	209	96	91	74	96	87	169	177	137
ΔE	0.06	0.09	0.22	0.59	0.54	0.27	0.17	0.0008	0.03	0.17	0.05	0.03	0.14	0.01	0.03	0.06	0.10
N_r	537	705	638	571	672	571	504	638	873	739	705	571	739	672	672	739	571
ΔE	-0.003	-0.01	-0.005	-0.002	-0.01	-0.02	-0.02	-0.006	-0.03	-0.0007	-0.002	-0.02	-0.05	-0.02	-0.01	-0.001	-0.02

^a diamond

TABLE II. The total energy differences between KS(KLI) SCAN and SCAN with PBE orbitals of different grids. N_r is the number of radial grid points. $\Delta E = E_{\text{SCAN}}^{\text{KS(KLI)}} - E_{\text{SCAN}}^{\text{PBE orb.}}$. All energies are in eV.

centered spherical grids. The radial part of the spherical grid is dense near the nuclei, and is sparse away from the nuclei. The integration weights for the grid points in the sparse region would be larger than those in the dense region. Therefore a function with sharp features in regions away from the nuclei cannot be properly represented on the grid, and the error of integrations involving this function would be large. One needs larger grids in gKS meta-GGA calculations than those used in GGA calculations.

We find that the OEP meta-GGA is more sensitive to the real-space integration grid than the gKS meta-GGA. In the gKS case, the sensitivity to the grid shows up in the potential energy surface^{63,64} as spurious oscillations, but the sensitivity is not obvious in a single-point calculation. In the OEP case, a single-point calculation is enough to demonstrate the grid sensitivity by comparing the total energy. The total energy of the OEP meta-GGA is variationally minimized with respect to the charge density, but the total energy of the gKS meta-GGA is variationally minimized with respect to the orbitals. Since the gKS has bigger variational degrees of freedom, the gKS total energy should always be lower than the OEP total energy, and both should be lower than the meta-GGA total energy evaluated with non-variational orbitals. However, though the built-in integration grids in the BAND code are good enough for gKS calculations, they are not sufficient for an OEP calculation: the OEP total energy calculated with these grids is always higher than the total energy evaluated with PBE orbitals. For example, the best built-in grid in BAND for the Ne atom has 120 radial points, but at least 266 radial points are required for the SCAN OEP total energy to be lower than the SCAN total energy evaluated with PBE orbitals, and 504 radial points are required for the SCAN OEP total energy to converge with respect to the grid (error < 0.01 meV). The total energy is not sensitive to the number of angular grid points. Table II lists the total energy differences using different grids.

The OEP v_{xc} of the Ne atom, Ar₂ dimer, and bulk Si (along the Si-Si bond) are plotted in Figs. 6, 7, and 8. The OEP v_{xc} develops unnatural peaks close to nuclei when too few grid points are used. These peaks have a strong effect on the KS band gap and the total energy. For bulk Si with 134 points (dashed line in Fig. 8), the system becomes gapless.

The grid-dependence of the OEP meta-GGA is caused

by $\nabla \partial e_{\text{xc}} / \partial \tau_{\sigma}$ in Eq. (12). Figs. 6, 7, and 8 show that $\nabla \partial e_{\text{xc}} / \partial \tau_{\sigma}$ has very sharp oscillations both close to and away from the nucleus. The dots in these plots show the grid point locations when the calculation is done with a built-in grid in BAND. These grid points are sufficient for an gKS meta-GGA calculation since they are dense enough to properly describe the oscillations in α , but they are insufficient for an OEP meta-GGA calculation since the peaks in $\nabla \partial e_{\text{xc}} / \partial \tau_{\sigma}$ are much narrower than those of α .

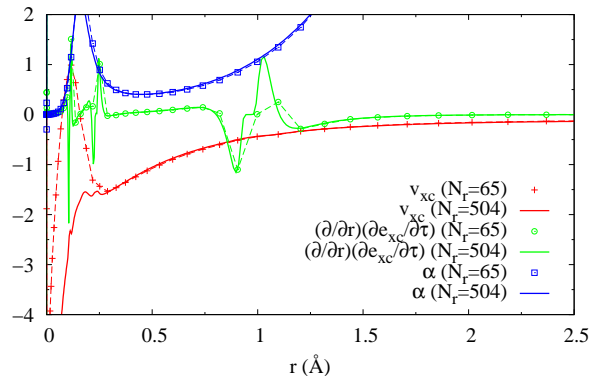


FIG. 6. (color online) The KS(ELP) SCAN v_{xc} (a.u.), the radial component of $\nabla \partial e_{\text{xc}} / \partial \tau$ (a.u.), and α of the Ne atom evaluated with two different grids. The solid lines are results obtained by using 504 radial grid points, and the dots and dashed lines are results obtained by using 65 radial points.

Fig. 9 shows $\nabla \partial e_{\text{xc}} / \partial \tau$ of the Ne atom for SCAN, TPSS, MS2, and MVS functionals. Though $\nabla \partial e_{\text{xc}} / \partial \tau$ of all functionals have oscillations, the sharpness of the peaks is different, and consequently the numbers of grid points required for convergence are also different: SCAN has very sharp peaks, and it requires 352 points to converge the total energy within 1% error; The peaks in MVS are broader, and it only requires 252 points to converge with the same error criterion.

The oscillations in $\nabla \partial e_{\text{xc}} / \partial \tau$ for SCAN, MS2 and MVS are centered at or close to $\alpha = 1$ in Fig. 9. All these functionals use α to incorporate the kinetic energy density into the functional, and their energy densities all have the form $e_{\text{xc}} = e_{\text{xc},1} + f(\alpha)(e_{\text{xc},0} - e_{\text{xc},1})$, where $e_{\text{xc},0}$ and $e_{\text{xc},1}$ are e_{xc} constructed for $\alpha = 0$ and $\alpha = 1$, and $f(\alpha)$ is an interpolation function that decreases mono-

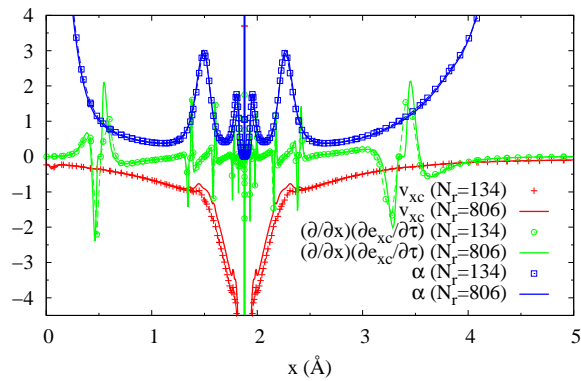


FIG. 7. (color online) The KS(KLI) SCAN v_{xc} (a.u.), the x component of $\nabla\partial e_{xc}/\partial\tau$ (a.u.), and α of the Ar dimer evaluated with two different grids, plotted along the Ar-Ar axis. The Ar atoms are located at $x = \pm 1.88\text{\AA}$, so that comparison with Ref. 63 is possible. Since the system is symmetric, only the $x \in [0, 4]$ part is plotted. The solid lines are results obtained by using 806 radial grid points, and the dots and dashed lines are results obtained by using 134 radial grid points.

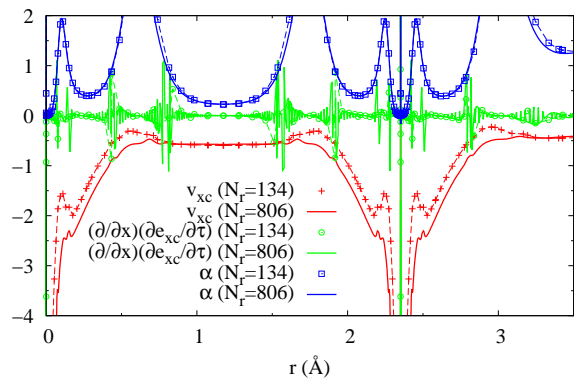


FIG. 8. (color online) The KS(KLI) SCAN v_{xc} (a.u.), the x component of $\nabla\partial e_{xc}/\partial\tau$ (a.u.), and α of bulk Si evaluated with two different grids, plotted along the Si-Si bond. The Si atoms are located at $r = 0$ and $r = 2.35\text{\AA}$. The solid lines are results obtained by using 571 radial grid points, and the dots and dashed lines are results obtained by using 134 radial grid points.

tonically with α from 1 at $\alpha = 0$ to 0 at $\alpha = 1$ to negative values for $\alpha > 1$. The oscillation in $\nabla\partial e_{xc}/\partial\tau$ then implies a peak in $df(\alpha)/d\alpha$. $\alpha = 1$ corresponds to the uniform electron gas limit, and the $f(\alpha)$ of SCAN and MS2 are constructed to have $d^2f(\alpha)/d\alpha^2 = 0$ there to recover the gradient expansion approximation³⁸. Therefore $df(\alpha)/d\alpha$ has a flat- or linearly-topped peak at $\alpha = 1$, which explains the oscillation. For MVS, $d^2f(\alpha)/d\alpha^2$ vanishes at $\alpha = 0.77$, and its oscillation in $\nabla\partial e_{xc}/\partial\tau$ occurs there. By choosing other functional forms for $f(\alpha)$, it is possible to get rid of the oscillations and the grid sensitivity. TPSS does not have this feature since it uses z instead of α .

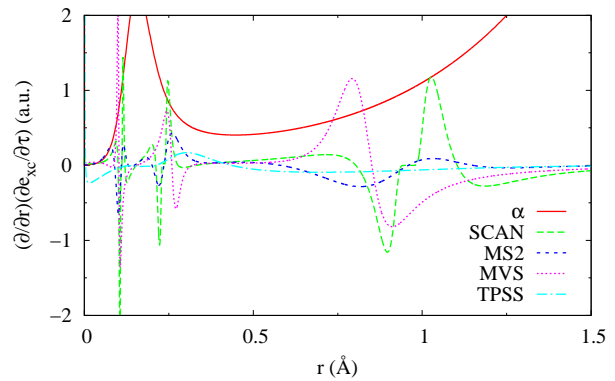


FIG. 9. (color online) The radial component of $\nabla\partial e_{xc}/\partial\tau$ of the Ne atom of different functionals. α 's of different functionals are similar, so only that of SCAN is plotted.

Even though a small grid cannot properly represent the oscillations in $\nabla\partial e_{xc}/\partial\tau$, Fig. 10 shows that the v_{xc} of the Slater approximation (which contains $\nabla\partial e_{xc}/\partial\tau$ explicitly) evaluated on a small grid is already similar to the KLI v_{xc} evaluated on a big grid. The KLI approximation is supposed to be an improvement over the Slater approximation, but it introduces big errors in v_{xc} when using a small grid. The grid sensitivity actually enters the OEP indirectly through the I integrals of Eq. (14). Since the Slater term contains $\nabla\partial e_{xc}/\partial\tau$, the I integrals cannot be done accurately with a small grid.

The gKS meta-GGA potential operator in Eq. (7) also contains $\nabla\partial e_{xc}/\partial\tau$, but the grid sensitivity of gKS is much lower than that of OEP. There is no contradiction since $\nabla\partial e_{xc}/\partial\tau$ does not have to be evaluated directly in gKS meta-GGA. Using integration by parts, the matrix elements $\langle \psi_{i\mathbf{k}\sigma} | \hat{v}_{xc,\sigma}^{\text{gKS}} | \psi_{j\mathbf{k}\sigma} \rangle$ becomes

$$\begin{aligned} & -\frac{1}{2} \int d^3r \psi_{i\mathbf{k}\sigma}^*(\mathbf{r}) \nabla \cdot \left[\frac{\partial e_{xc}}{\partial\tau_\sigma}(\mathbf{r}) \nabla \psi_{j\mathbf{k}\sigma}(\mathbf{r}) \right] \\ & = \frac{1}{2} \int d^3r \frac{\partial e_{xc}}{\partial\tau_\sigma}(\mathbf{r}) \nabla \psi_{i\mathbf{k}\sigma}^*(\mathbf{r}) \cdot \nabla \psi_{j\mathbf{k}\sigma}(\mathbf{r}), \quad (16) \end{aligned}$$

and $\partial e_{xc}/\partial\tau$ is less sensitive to the grid than $\nabla\partial e_{xc}/\partial\tau$. The grid sensitivity of the OEP is also expected to show up in the time-dependent density-functional theory (TDDFT)⁶⁵ with a meta-GGA xc kernel.

Aside from the grid problem, we find that the OEP meta-GGA in general needs more self-consistent-field (SCF) cycles to reach convergence than the gKS meta-GGA. For small gap materials, the OEPs of some meta-GGA functionals do not converge, while the corresponding gKS calculations converge normally. We tested SCAN, MS2, MVS, and TPSS functionals, and SCAN has the least convergence problem.

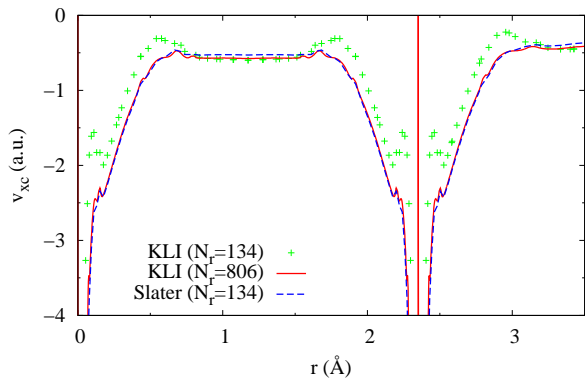


FIG. 10. (color online) KS(KLI) SCAN v_{xc} of bulk Si along the Si-Si bond. The Si atoms are located at $r = 0$ and $r = 2.35\text{\AA}$.

V. CONCLUSION

In conclusion, we implemented the ELP and the KLI approximations for the OEP meta-GGA of periodic systems, with which we study the meta-GGA band gaps of 20 semiconductors and insulators. Comparing with the GGA band gaps, the new SCAN meta-GGA in a generalized Kohn-Sham scheme is found to improve the band gaps over the GGA band gaps. The non-empirical SCAN meta-GGA outperforms the non-empirical PBE GGA, not only for diversely-bonded materials near equilibrium¹², but also for the band gaps of solids. The improvement is achieved without using the expensive exact exchange, as in fourth-rung hybrid functionals. For materials wrongly predicted to be gapless in GGA, the result⁵⁷ of $\beta\text{-MnO}_2$ with SCAN shows that meta-GGAs can open the gap.

Consider the ratio of the calculated to the experimental energy gap. For the 17 solids of Table I, this ratio varies from 0.35 to 0.79 with an average of 0.60 for the PBE GGA, from 0.53 to 0.94 with an average of 0.73 for the

SCAN meta-GGA, and from 0.72 to 1.07 with an average of 0.89 for the HSE hybrid functional. The ratio improves uniformly from PBE to SCAN to HSE. While the hybrid functional is more accurate for the gap than SCAN is, it is also more empirical and more computationally expensive.

For periodic systems, the OEP or ungeneralized Kohn-Sham v_{xc} 's of meta-GGAs are close to the GGA v_{xc} 's, and they only differ in small details. Consequently the OEP meta-GGA gaps (like the OEP EXX+RPA gaps where available) are not improved significantly over the GGA gaps, and the band structures of OEP meta-GGAs are similar to those of GGAs. We think it is likely that the band gap and band structure in the exact Kohn-Sham potential are close to those of GGA and OEP meta-GGA (and of the OEP hybrid) in periodic systems. Aside from the band gap, the gKS meta-GGA band structures are also similar to the GGA band structures.

Due to the sharp features in $\nabla\partial e_{xc}/\partial\tau_\sigma$, the OEP meta-GGA is sensitive to the real-space grid used in computation, more so than the gKS meta-GGA. Different meta-GGAs have different requirements for the minimal grid, and in general SCAN needs the biggest grid to converge of the meta-GGAs tested in this work. TDDFT with meta-GGA xc kernels is also expected to show this grid sensitivity. It is possible to avoid the grid sensitivity in the design of the functional, although this may interfere with the satisfaction of some exact conditions.

ACKNOWLEDGEMENTS

ZY, JS and JPP are supported by the National Science Foundation(Grant No. DMR-1305135). HP, JS, and JPP are also supported by the Center for the Computational Design of Functional Layered Materials, an Energy Frontier Research Center (EFRC) funded by the U.S. Department of Energy, Office of Science, Basic Energy Sciences under Award No. DE-SC0012575. The EFRC grant contributed to the computational aspects of this work. We thank Kieron Burke for suggestions on the manuscript.

¹ P. Y. Yu and M. Cardona, *Fundamentals of semiconductors: physics and materials properties* (Springer, Berlin, 2010).

² L. Hedin, Phys. Rev. **139**, A796 (1965).

³ P. Hohenberg and W. Kohn, Phys. Rev. **136**, B864 (1964).

⁴ W. Kohn and L. J. Sham, Phys. Rev. **140**, A1133 (1965).

⁵ C. Fiolhais, F. Nogueira, and M. Marques, eds., *A primer in density functional theory*, Lecture notes in physics (Springer, Berlin, 2003).

⁶ J. P. Perdew and K. Schmidt, in *Density functional theory and its application to materials*, edited by V. van Doren, C. van Alsenoy, and P. Geerlings (AIP Press, New York, 2001).

⁷ J. P. Perdew, R. G. Parr, M. Levy, and J. L. J. Balduz, Phys. Rev. Lett. **49**, 1691 (1982).

⁸ A. Seidl, A. Görling, G. P. Vogl, J. A. Majewski, and M. Levy, Phys. Rev. B **53**, 3764 (1996).

⁹ M. E. Casida, Phys. Rev. B **59**, 4694 (1999).

¹⁰ R. Neumann, R. H. Nobes, and N. C. Handy, Mol. Phys. **87**, 1 (1996).

¹¹ Y. Zhao and D. G. Truhlar, J. Chem. Phys. **130**, 074103 (2009).

¹² J. Sun, A. Ruzsinszky, and J. P. Perdew, Phys. Rev. Lett. **115**, 036402 (2015).

¹³ J. Sun, R. C. Remsing, Y. Zhang, Z. Sun, A. Ruzsinszky, H. Peng, Z. Yang, A. Paul, U. Waghmare, X. Wu, M. L. Klein, and J. P. Perdew, Nature Chem., to appear.

¹⁴ J. P. Perdew, A. Ruzsinszky, G. I. Csonka, O. A. Vydrov, G. E. Scuseria, L. A. Constantin, X. Zhou, and K. Burke, Phys. Rev. Lett. **100**, 136406 (2008).

¹⁵ R. T. Sharp and G. K. Horton, Phys. Rev. **90**, 317 (1953).

- ¹⁶ J. D. Talman and W. F. Shadwick, Phys. Rev. A **14**, 36 (1976).
- ¹⁷ A. V. Arbuznikov and M. Kaupp, Chem. Phys. Lett. **381**, 495 (2003).
- ¹⁸ F. G. Eich and M. Hellgren, J. Chem. Phys. **141**, 224107 (2014).
- ¹⁹ F. Tran and P. Blaha, Phys. Rev. Lett. **102**, 226401 (2009).
- ²⁰ A. V. Kosobutsky and A. B. Gordienko, Phys. Solid State **57**, 1972 (2015).
- ²¹ S. Ivanov, S. Hirata, and R. J. Bartlett, Phys. Rev. Lett. **83**, 5455 (1999).
- ²² F. Della Sala and A. Goerling, J. Chem. Phys. **115**, 5718 (2001).
- ²³ V. N. Staroverov, G. E. Scuseria, and E. R. Davidson, J. Chem. Phys. **125**, 081104 (2006).
- ²⁴ A. F. Izmaylov, V. N. Staroverov, G. E. Scuseria, E. R. Davidson, G. Stoltz, and E. Cancès, J. Chem. Phys. **126**, 084107 (2007).
- ²⁵ O. V. Gritsenko and E. J. Baerends, Phys. Rev. A **64**, 042506 (2001).
- ²⁶ M. Grüning, O. V. Gritsenko, and E. J. Baerends, J. Chem. Phys. **116**, 6435 (2002).
- ²⁷ J. B. Krieger, Y. Li, and G. J. Iafrate, Phys. Rev. A **45**, 101 (1992).
- ²⁸ J. C. Slater, Phys. Rev. **81**, 385 (1951).
- ²⁹ P. E. Blöchl, Phys. Rev. B **50**, 17953 (1994).
- ³⁰ G. Kresse and D. Joubert, Phys. Rev. B **59**, 1758 (1999).
- ³¹ G. te Velde and E. J. Baerends, Phys. Rev. B **44**, 7888 (1991).
- ³² G. Wiesenekker and E. J. Baerends, J. Phys.: Cond. Matt. **3**, 6721 (1991).
- ³³ M. Franchini, P. H. T. Philipsen, and L. Visscher, J. Comput. Chem. **34**, 1818 (2013).
- ³⁴ M. Franchini, P. H. T. Philipsen, E. van Lenthe, and L. Visscher, J. Chem. Theory Comput. **10**, 1994 (2014).
- ³⁵ P. H. T. Philipsen, G. te Velde, E. J. Baerends, J. A. Berger, P. L. de Boeij, M. Franchini, J. A. Groeneveld, E. S. Kadantsev, R. Klooster, F. Kootstra, P. Romaniello, D. G. Skachkov, J. G. Snijders, C. J. O. Verzipl, G. Wiesenekker, and T. Ziegler, “Band2014 (a modified version is used),” SCM, Theoretical Chemistry, Vrije Universiteit, Amsterdam, The Netherlands, <http://www.scm.com>.
- ³⁶ A. D. Becke, J. Chem. Phys. **88**, 2547 (1988).
- ³⁷ H. J. Monkhorst and J. D. Pack, Phys. Rev. B **13**, 5188 (1976).
- ³⁸ J. Sun, B. Xiao, and A. Ruzsinszky, J. Chem. Phys. **137**, 051101 (2012).
- ³⁹ J. Sun, R. Haunschild, B. Xiao, I. W. Bulik, G. E. Scuseria, and J. P. Perdew, J. Chem. Phys. **138**, 044113 (2013).
- ⁴⁰ J. Sun, J. P. Perdew, and A. Ruzsinszky, Proc. Nat. Acad. Sci. **112**, 685 (2014).
- ⁴¹ J. Tao, J. P. Perdew, V. N. Staroverov, and G. E. Scuseria, Phys. Rev. Lett. **91**, 146401 (2003).
- ⁴² J. P. Perdew, K. Burke, and M. Ernzerhof, Phys. Rev. Lett. **77**, 3865 (1996).
- ⁴³ E. van Lenthe and E. J. Baerends, J. Comput. Chem. **24**, 1142 (2003).
- ⁴⁴ P. H. T. Philipsen, E. van Lenthe, J. G. Snijders, and E. J. Baerends, Phys. Rev. B **56**, 13556 (1997).
- ⁴⁵ G. B. Bachelet and N. E. Christensen, Phys. Rev. B **31**, 879 (1985).
- ⁴⁶ I. G. Ryabinkin and V. N. Staroverov, J. Chem. Phys. **137**, 164113 (2012).
- ⁴⁷ O. Madelung, *Semiconductors: Data Handbook* (Springer, 2004).
- ⁴⁸ M. P. Surh, S. G. Louie, and M. L. Cohen, Phys. Rev. B **43**, 9126 (1991).
- ⁴⁹ J. Heyd, G. E. Scuseria, and M. Ernzerhof, J. Chem. Phys. **118**, 8207 (2003).
- ⁵⁰ J. Heyd, J. E. Peralta, G. E. Scuseria, and R. L. Martin, J. Chem. Phys. **123**, 174101 (2005).
- ⁵¹ J. Heyd, G. E. Scuseria, and M. Ernzerhof, J. Chem. Phys. **124**, 219906 (2006).
- ⁵² G. Kresse and J. Hafner, Phys. Rev. B **47**, 558 (1993).
- ⁵³ G. Kresse and J. Hafner, Phys. Rev. B **49**, 14251 (1994).
- ⁵⁴ G. Kresse and J. Furthmüller, Comput. Mat. Sci. **6**, 15 (1996).
- ⁵⁵ G. Kresse and J. Furthmüller, Phys. Rev. B **54**, 11169 (1996).
- ⁵⁶ M. Grüning, A. Marini, and A. Rubio, J. Chem. Phys. **124**, 154108 (2006).
- ⁵⁷ D. A. Kitchaev, H. Peng, Y. Liu, J. Sun, J. P. Perdew, and G. Ceder, Phys. Rev. B **93**, 045132 (2016).
- ⁵⁸ R. Peverati and D. G. Truhlar, J. Chem. Phys. **136**, 134704 (2012).
- ⁵⁹ J. F. Janak, Phys. Rev. B **18**, 7165 (1978).
- ⁶⁰ P. Mori-Sánchez, A. J. Cohen, and W. Yang, Phys. Rev. Lett. **100**, 146401 (2008).
- ⁶¹ W. Yang, A. J. Cohen, and P. Mori-Sánchez, J. Chem. Phys. **136**, 204111 (2012).
- ⁶² R. W. Godby, M. Schlüter, and L. J. Sham, Phys. Rev. Lett. **56**, 2415 (1986).
- ⁶³ E. R. Johnson, A. D. Becke, C. D. Sherrill, and G. A. DiLabio, J. Chem. Phys. **131**, 034111 (2009).
- ⁶⁴ E. R. Johnson, R. A. Wolkow, and G. A. DiLabio, Chem. Phys. Lett. **394**, 334 (2004).
- ⁶⁵ E. Runge and E. K. U. Gross, Phys. Rev. Lett. **52**, 997 (1984).